Dynamic Characteristics of Integral Gain Changeable Digital Control DC-DC Converter for Suppression of Output Capacitance

Kazuhiro Kajiwara*, Hidenobu Tajima*, Hidenori Maruta*, Fujio Kurokawa*, Ilhami Colak**

* Graduate School of Engineering, Nagasaki University, 1-14 Bunkyo-machi,

Nagasaki, 852-8521, Japan

** Faculty of Engineering and Architecture, Gelisim University, Cihangir quarter

Şehit Jandarma Komando Er Hakan Öner Street. No:1 Avcılar, Istanbul, Turkey

(bb52311101@cc.nagasaki-u.ac.jp, amsky1306@gmail.com, hmaruta@nagasaki-u.ac.jp

fkurokaw@nagasaki-u.ac.jp, icolak@gelisim.edu.tr)

‡Corresponding Author; Kazuhiro Kajiwara, Graduate School of Engineering,

Nagasaki University, 1-14 Bunkyo-machi, Nagasaki, 852-8521, Japan,

Tel: +81 95 819 2553, bb52311101@cc.nagasaki-u.ac.jp

Received: 01.02.2016 Accepted:10.02.2016

Abstract- Stability of power converters has become more and more important in hybrid green energy systems because of its difficulties to maintain a stable dc-bus. This paper presents dynamic characteristics of a digital integral gain changeable control dc-dc converter to realize high stability with suppression of the output capacitance. The integral gain changeable control method uses a variable integral gain, which is changed by the value of load current. The stability analysis is conducted by Bode diagrams. It is shown that the transient response and stability of the integral gain changeable method are better than the conventional fixed integral gain control method even if the output capacitance is smaller than the conventional method. Simulation and experimental results show the effectiveness of our concept.

Keywords dc-dc converter; digital control; integral gain; stability analysis; transient response; output capacitance.

1. Introduction

Global emissions of carbon dioxide have more than doubled compared with 1973 with increasing the power consumption, [1]. The hybrid green energy system, which consists of solar, wind power and so forth as shown in Fig. 1, has been attracted to reduce global emissions of carbon dioxide [2]-[4]. Green energy is connected to the dc-bus through ac-dc and dc-dc converters. Since green energy sources are affected by weather conditions, the power generation amount is extremely varied by time. Battery energy storage is utilized to regulate the power generation amount in a hybrid system. Although this system is effective for energy saving, it is difficult to obtain stable dc-bus enough [5]-[7]. The dc-dc converter connected to the dc load should therefore have wide regulation characteristics to address input voltage fluctuations.

Moreover, a lot of dc-dc converters are connected with home electrical appliances and LEDs as the dc-load at home in this system [8]. The energy saving mode is expected to increase in electronic equipment. A dc-dc converter creates a discontinuous conduction mode (DCM) in this mode. An output voltage of the dc-dc converter is unusually increased in DCM. Also, a large transient response occurs when the operation of electronic equipment changes from DCM to the continuous conduction mode (CCM). Additionally, dc-dc

converters in this field are required downsizing [9], [10]. Therefore, control methods for dc-dc converters are required a sufficient stability margin with a small output capacitance

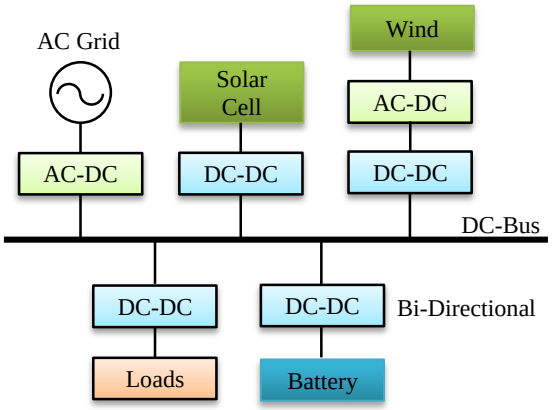

Figure 1. Schematic diagram of hybrid green energy system.

in the wide range of input voltage and load.

Some gain tuning methods based on the PID control have been already studied to realize high stability [11]-[16]. In [16], a simple integral gain changeable control method has been presented. The integral gain is desirable to be small value to obtain enough stability of system when the inductor current is on CCM. On the other hand, the large integral gain is necessary for DCM to suppress the increase of the output voltage. Minimum required values of the integral gain are calculated from an analysis formula of a stabilization range of the output voltage based on the I (Integral) control. This method can obtain both wide regulation characteristics and a quick response by changing the integral gain based on the load current value even if the input voltage is changed. [16] has reported the design method of integral gain changeable function. To verify the further effectiveness of this control in the hybrid system, the stability analysis and the circuit design including the value of output capacitance should be investigated.

This paper analyses dynamic characteristics of the digital integral gain changeable control, and presents its transient response. The stability analysis shows that the digital integral gain changeable control method has high stability compared with the fixed gain control method. Furthermore, this method shows a superior transient response with high stability even if a smaller output capacitance is used.

2. Operation Principle of Integral Gain Changeable Control

Isolated dc-dc converters like forward or bridge type are usually connected to the dc load in a hybrid system. This paper uses a non-isolated buck converter by modelling an isolated dc-dc converter. Figure 2 shows the circuit configuration of digital control dc-dc converter with the existing integral gain changeable control method. E_i is the input voltage, e_o is the output voltage, i_L is the reactor current, I_o is the load current, T_r is the main switch, D is the fly wheel diode, L is the energy storage reactor, C is the output capacitor, R is the load and R_S is the sensing resister for I_o. e_o is sent to the pre-amplifier and the A-D converter

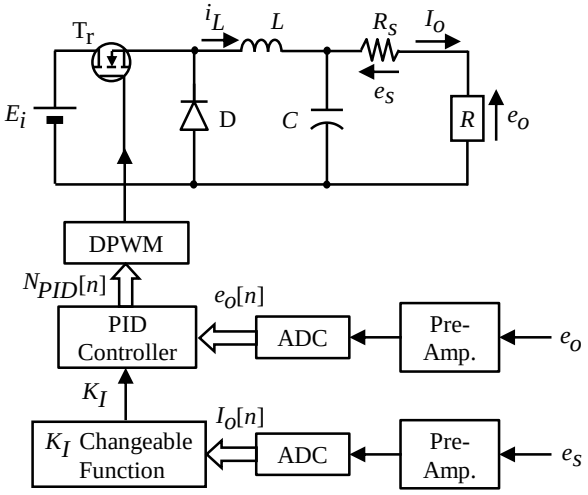

Figure 2. Digital control buck converter with existing integral gain changeable control method.

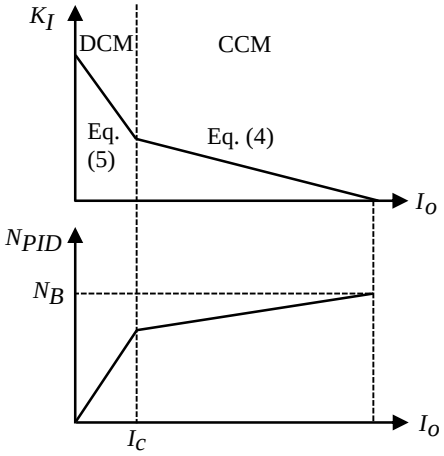

Figure 3. Stabilization range of e_o based on I control.

(ADC). The digital value of output voltage $e_o[n]$ is obtained as follows:

$$e_o[n] = A_{eo} \cdot G_{AD} \cdot e_o \tag{1}$$

where A_{eo} and G_{AD} are gains of the pre-amplifier and the ADC, and n denotes n-th switching period.

$e_o[n]$ is fed into the PID controller. Equation (2) represents the PID control calculation value $N_{PID}[n]$.

$$\begin{aligned} N_{PID}[n] = N_B &- K_P(e_o[n-1] - N_R) \\ &- K_I \Sigma(e_o[n-1] - N_R) \\ &- K_D(e_o[n-1] - e_o[n-2]) \end{aligned} \tag{2}$$

where N_B is the digital bias value to determine the operation point of buck converter, N_R is the digital value of desired output voltage. Also, K_P, K_I and K_D are proportional, integral and derivative coefficients.

The on-time T_{on} is obtained from $N_{PID}[n]$ in the digital pulse width modulation (DPWM). The relationship between T_{on} and $N_{PID}[n]$ is derived as follows:

$$\frac{T_{on}}{T_s} = \frac{N_{PID}[n]}{N_{Ts}} \tag{3}$$

where N_{Ts} is the numerical digital value corresponding to the switching period T_s.

The existing method changes K_I to obtain high stability in a wide operation range. A small value of K_I is desirable in CCM to keep an enough stability margin, while a large value of K_I is necessary to remove the steady-state error of e_o in DCM. K_I changeable function in Fig. 2 therefore calculates K_I by using the value of I_o in every switching period. According to [16], the minimum required value of K_I for the buck converter is calculated by the analysis of the stabilization range of e_o based on I control as shown in Fig. 3. I_c is the critical current. When N_{PID} is less than N_B in the steady-state, the analysis formula in CCM is represented as follows:

$$K_I \geq \frac{N_B}{2^Q - 1} - \frac{N_{Ts}}{E_i\left(2^Q - 1\right)}\left(rI_o + E_o{}^*\right). \tag{4}$$

In DCM,

$$K_I \geq \frac{N_B}{2^Q - 1} - \frac{2LN_{Ts}I_o}{T_{on}E_i\left(2^Q - 1\right)\left\{\left(E_i / E_o{}^*\right) - 1\right\}} \tag{5}$$

where Q is a bit number of the I control part, $E_o{}^*$ is the desired output voltage and r is the internal loss of buck converter.

When Eqs. (4) and (5) are used for calculation of K_I, K_I changeable function becomes complex because the calculation part has to be switched between CCM and DCM. Furthermore, the minimum required value of K_I is determined by E_i and I_o. It is necessary for the detection of E_i to add an ADC and a sensing circuit in the existing method. Therefore, K_I changeable function is implemented by a single logarithm function to realize a simple calculation as follows:

$$K_I = \alpha \cdot \ln\left(I_o\right) + \beta \tag{6}$$

where α and β are constant values. Since the detail design of K_I changeable function has been already discussed in [16], it is not reviewed again here.

3. Circuit Configuration and Transfer Function

Figure 4 shows the continuous averaged model of buck converter. The transfer function is represented by Fig. 5 using small variations Δe_o, Δe_i, ΔR and ΔT_{on} [17]. $G(s)$

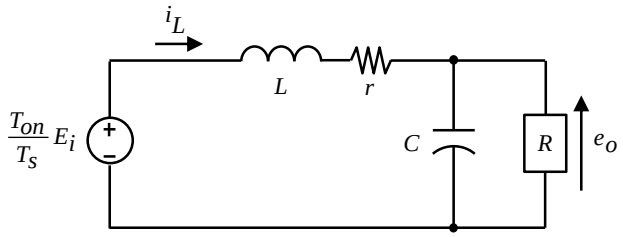

Figure 4. Continuous averaged model of buck converter.

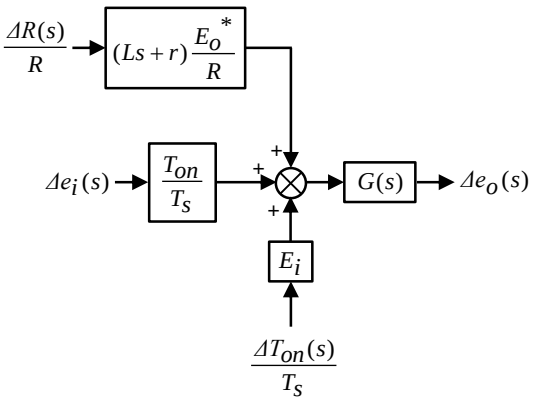

Figure 5. Block diagram of transfer function in buck converter.

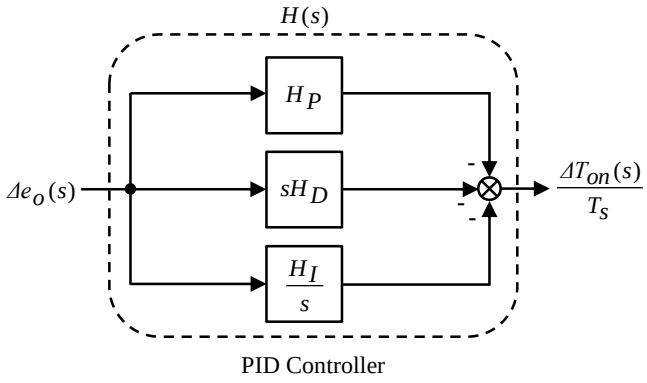

Figure 6. Block diagram of transfer function in PID controller.

is the transfer function of buck converter and represented by a second order output filter as follows:

$$G(s) = \frac{1/LC}{s^2 + s\left(\frac{1}{CR} + \frac{r}{L}\right) + \frac{1}{LC}\left(1 + \frac{r}{R}\right)} \tag{7}$$

where s is the Laplace operator.

Figure 5 illustrates the block diagram of transfer function in the PID controller. The duty ratio T_{on}/T_S is determined by N_{PID}. When e_o is infinitesimally changed, N_{PID} and T_{on} are also changed. Thereby, Eq. (8) is derived by taking account of ΔT_{on} and Δe_o in Eqs. (2) and (3) as follows:

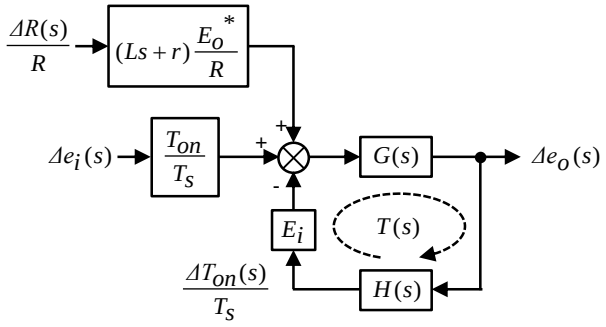

Figure 7. Block diagram of transfer function in digital control buck converter.

$$\frac{\Delta T_{on}(s)}{T_S} = -H(s)\cdot \Delta e_o(s) \tag{8}$$

where $H(s)$ is the transfer function of PID controller and expressed as follows:

$$H(s) = \frac{\Delta T_{on}(s)/T_S}{e_o(s)} = \left(H_P + \frac{H_I}{s} + sH_D \right) e^{-s(\tau_1+\tau_2)} \tag{9}$$

where τ_1 is the delay time of digital controller which is normally one switching period, and τ_2 is the time constant of the anti-aliasing filter for e_o. Also, H_P, H_I, and H_D are proportional, integral and derivative gains, and represented by Eqs. (10) through (12).

$$H_P = \frac{K_P A_{eo} G_{AD}}{N_{Ts}} \tag{10}$$

$$H_I = \frac{K_I A_{eo} G_{AD}}{N_{Ts}\cdot T_S} \tag{11}$$

$$H_D = \frac{K_D A_{eo} G_{AD} T_S}{N_{Ts}} \tag{12}$$

Here, $e^{-s(\tau_1+\tau_2)}$ is approximated as

$$e^{-s(\tau_1+\tau_2)} \approx \frac{1}{1+s(\tau_1+\tau_2)}. \tag{13}$$

Equation (14) is derived by substituting (13) into (9).

$$H(s) = \frac{s^2 H_D + sH_P + H_I}{s^2(\tau_1+\tau_2)+s} \tag{14}$$

From Figs. 5 and 6, the block diagram of the transfer function in the buck converter digital control buck converter is obtained as Fig. 7. The stability of the system is verified by the open loop transfer function $T(s)$ between $\Delta e_o(s)$ and $\Delta T_{on}(s)$. T(s) is represented as follows:

$$T(s) = E_i \cdot G(s)\cdot H(s). \tag{15}$$

4. Evaluation of Dynamic Characteristics

4.1. Stability Analysis

The stability analysis of the gain changeable control is verified by using the digital control buck converter, in which parameters are E_i = 16-24 V (±20% of 20 V), $E_o{}^*$ = 5 V, T_S = τ_1 = 10 μs, L = 183 μH, τ_2 = 8.2 μs and N_{Ts} = 2000. The rated load current is 1 A. I_c = 0.1 A, r = 0.42 Ω, R_s = 0.05 Ω, A_{eo} = 0.25, G_{AD} = 400, H_P is 0.05 V^{-1} and H_D is 0.5 μs·V^{-1}. According to [16], K_I changeable function is obtained as in Fig. 8 and represented by Eq. (16) when N_B is equal to 676.

$$K_I = -0.002\cdot \ln(I_o) + 0.008. \tag{16}$$

K_I becomes small in CCM and becomes large in DCM from Fig. 8 and Eq. (16). On the other hand, K_I is set to 0.022 to obtain wide regulation characteristics against E_i and I_o variations in the conventional gain fixed method. H_I is 110 $s^{-1}\cdot V^{-1}$ in the conventional method.

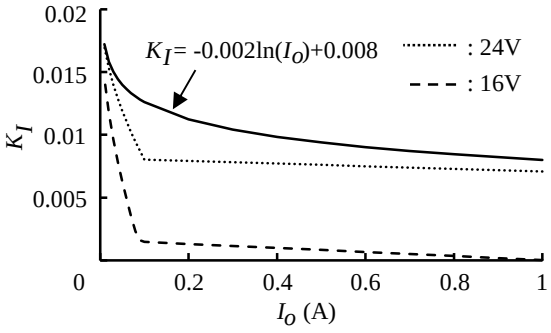

Figure 8. K_I changeable function.

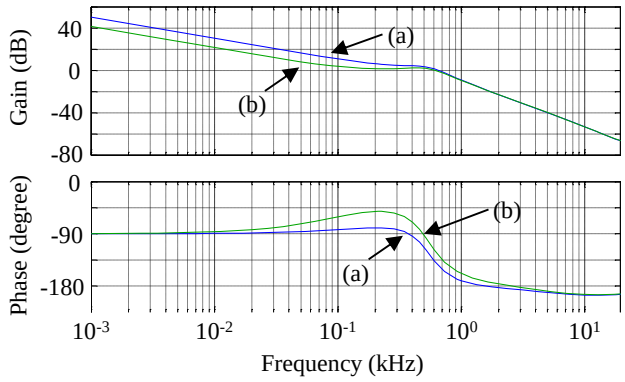

Figure 9. Bode diagrams of $T(s)$ when E_i is 20 V and C is 500 μF. (a) Conventional method. (b) Gain changeable method.

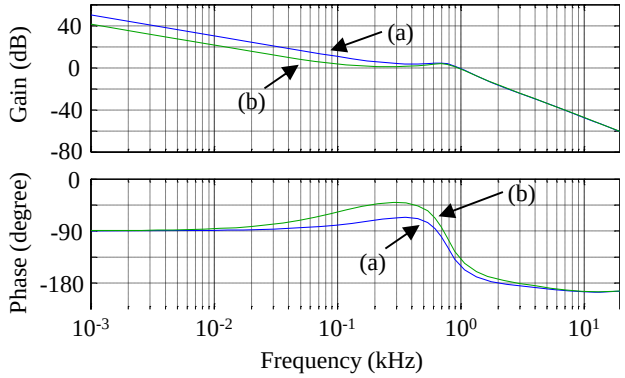

Figure 10. Bode diagrams of $T(s)$ when E_i is 20 V and C is 250 μF. (a) Conventional method. (b) Gain changeable method.

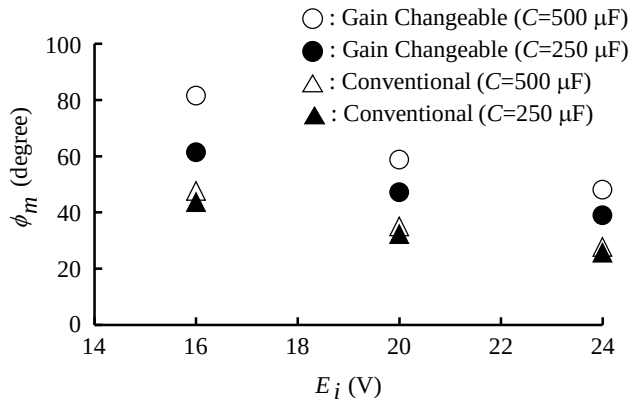

Figure 11. Summary of ϕ_m.

At first, Bode diagrams of $T(s)$ in the integral gain changeable and conventional methods are investigated by using MATLAB. R is 5 Ω in Bode diagrams. Figure 9 shows Bode diagrams when E_i is 20 V and C is 500 μF. The blue line shows the conventional method and the green line shows the gain changeable method. Frequency characteristics are shown from 1 Hz to 19.4 kHz, which is the cut off frequency of anti-aliasing filter. Since R is 5 Ω and $E_o{}^*$ is 5 V, I_o is 1 A. When I_o is 1 A, K_I is 0.008 and H_I is 40 $s^{-1}{\cdot}V^{-1}$ in the integral gain changeable control method. As shown in Fig. 9, the phase margin ϕ_m is 35 degree in the conventional method and 59 degree in the gain changeable method. ϕ_m is improved by the gain changeable method because H_I is smaller than the conventional method.

Figure 10 shows Bode diagrams when E_i is 20 V and C is changed to 250 μF. In this case, ϕ_m is 32 degree in the conventional method and 47 degree in the gain changeable method. It is confirmed that the gain changeable method has higher stability compared with the conventional method in spite of using a smaller value of C.

Figure 11 shows the summary of ϕ_m when E_i and C are changed. The gain changeable method has a superior stability to the conventional method in the wide range of E_i. It is also shown that C can be suppressed by 50%. Additionally, the gain changeable method can quickly change K_I by detection of I_o in the load step change. Therefore, both a quick response and high stability are obtained with a small value of C.

4.2. Transient Response Based on Experimental Results

Simulation results are obtained by a circuit simulator PSIM using the circuit model in Section 3. In the experimental circuit, the integral gain changeable control is performed by a DSP TMS320C6713-225. The DPWM is implemented by a XILINX Virtex-5 FPGA. As evaluation parameters, t_{cv} is the time that e_o converges within 1% from $E_o{}^*$. δ_{eo_under} and δ_{iL_over} are the undershoot of e_o and the overshoot of i_L.

Figure 12 shows the transient response of the conventional method when E_i is 20V, C is 530 μF and the load step change is from 0.05 A to 1 A. H_P is 0.05 V^{-1}, H_I is 110 $s^{-1}{\cdot}V^{-1}$ and H_D is 0.5 $\mu s{\cdot}V^{-1}$. It is found that the and the experimental results are well matched. The experimental result shows that t_{cv} is 5.1 ms, δ_{eo_under} and δ_{iL_over} are 840 mV and 960 mA.

Figure 13 shows the transient response of the gain changeable method when E_i is 20 V, C is 240 μF and a load step change is from 0.05 A to 1 A. H_P and H_D are the same values with the conventional method. As shown in Fig. 13, K_I is 0.014 when I_o is 0.05A. After a load step change to 1 A, K_I is instantaneously changed to 0.008. Thus, H_I is shifted from 70 $s^{-1}{\cdot}V^{-1}$ to 40 $s^{-1}{\cdot}V^{-1}$ in the transient response. As mentioned above, high stability is realized by decreasing H_I in the CCM. t_{cv} is 3.4 ms, δ_{eo_under} is 620 mV and

δ_{iL_over} is 620 mA in this case. As a result, the gain changeable method using a smaller output capacitance shows that t_{cv}, δ_{eo_under} and δ_{iL_over} are suppressed by 33%, 26%, and 35%, respectively compared with the conventional method in Fig. 12.

The summary of transient response in experimental results is shown in Fig, 14. δ_{eo_under} and δ_{iL_over} are improved by the gain changeable method in a wide range of E_i. When E_i is 16V, t_{cv} is longer than the conventional method. Since ϕ_m is increased by decreasing E_i, very high stability is obtained. The response speed is impaired in this situation. The gain changeable method using 240 μF has better transient response compared with the conventional method using 530 μF capacitance. It is verified that the gain changeable method can suppress the output capacitance with the quick response and keeping high stability.

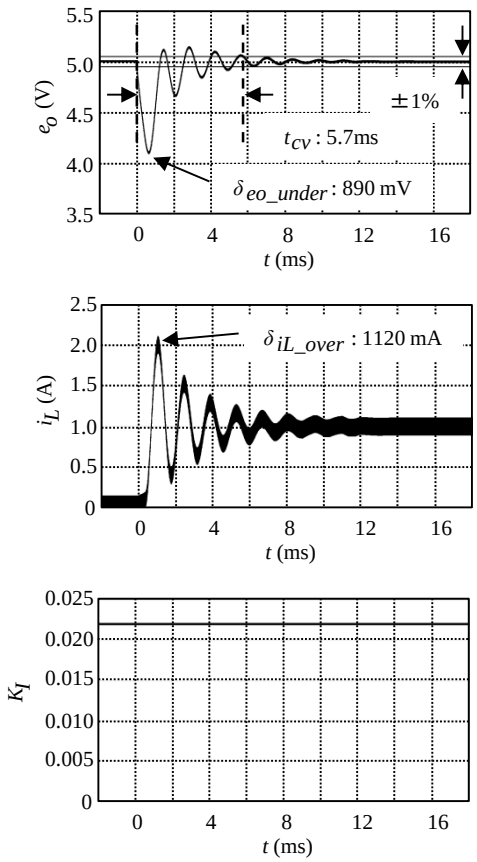

(a) Simulation result.

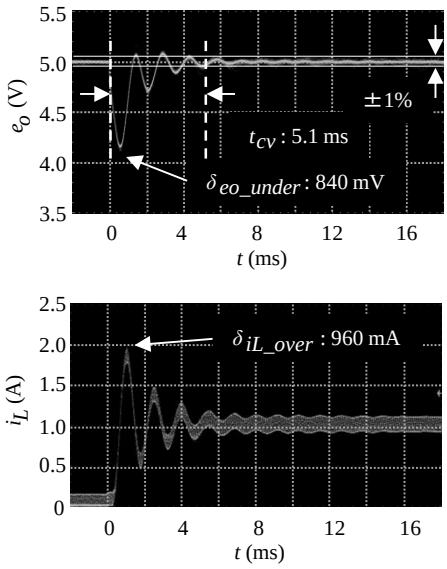

(b) Experimental result.

Figure 12. Transient response of conventional method in step change of I_O from 0.05A to 1A when C is 530 μF.

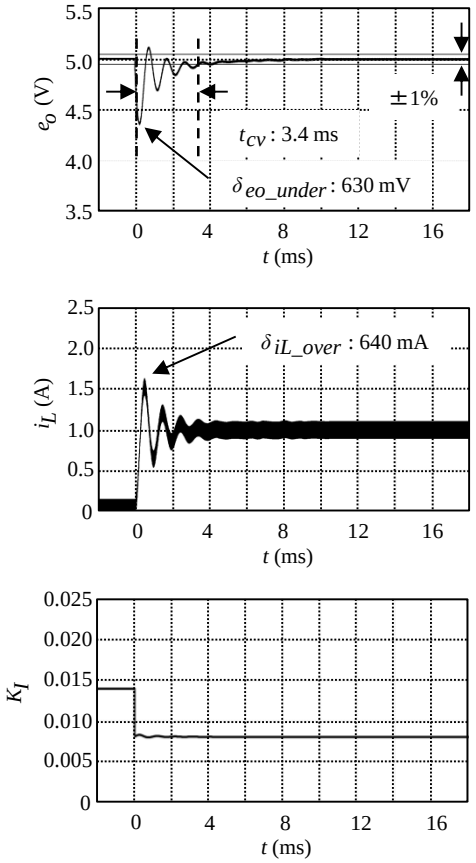

(a) Simulation result.

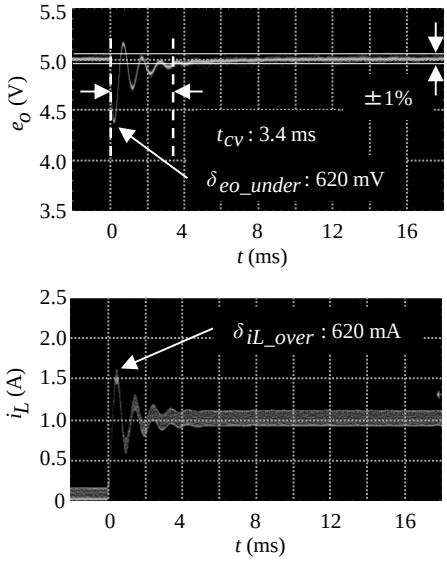

(b) Experimental result.

Figure 13. Transient response of integral gain changeable method in step change of I_o from 0.05A to 1A when C is 240 μF.

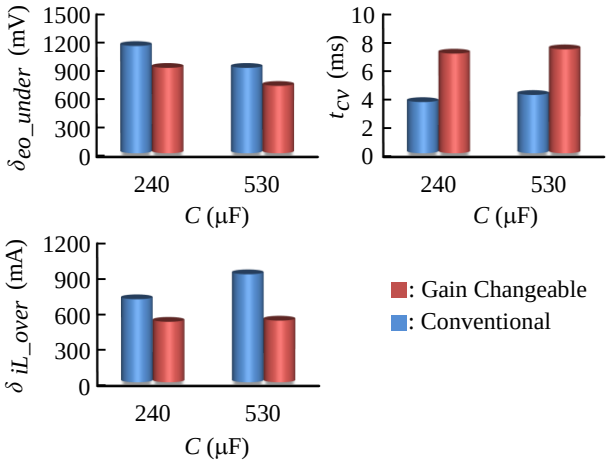

(a) E_i = 16 V

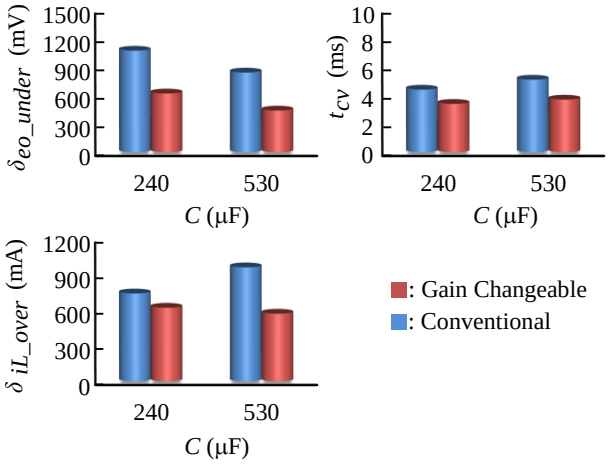

(b) E_i = 20 V

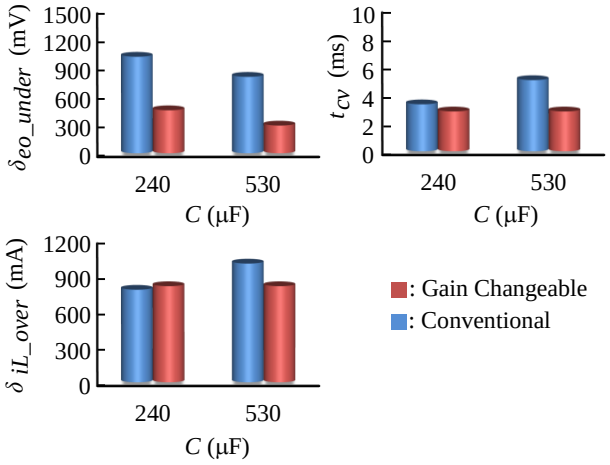

(c) E_i = 24 V

Figure 14. Summary of transient response in experimental results.

5. Conclusion

Dynamic characteristics of the integral gain changeable digital control dc-dc converter are presented in this paper. It

is concluded from the stability analysis by Bode diagrams, the integral gain changeable control method has high stability with a smaller output capacitance compared with the conventional method in the wide range of input voltage. Moreover, it is revealed that a superior transient response is obtained by the integral gain changeable method even if a small output capacitance is used. Therefore, this method can contribute to stability improvement and miniaturization of dc-dc converters. In near future, we will apply the integral gain changeable control method to the forward type or bridge type converter to offer a practical design.

References

[1] Key World Energy Statistics 2015, International Energy Agency, Nov. 2015.

[2] H. H. Abdeltawab and Y. A. I. Mohamed, "Market-oriented energy management of a hybrid wind-battery energy storage system via model predictive control with constraint optimizer," IEEE Trans. on Industrial Electronics, vol. 62, no. 11, pp. 6658–6670, Nov. 2015.

[3] D. B. W. Abeywardana, B. Hredzak, and V. G. Agelidis, "Single-phase grid-connected $LiFePO_4$ battery-supercapacitor hybrid energy storage system with interleaved boost inverter," IEEE Trans. on Power Electronics, vol. 30, no. 10, pp. 5591–5604, Oct. 2015.

[4] F. Zhang, Y. Yang, C. Ji, W. Wei, Y. Chen, C. Meng, Z. Jin, and G. Zhang, "Power management strategy research for dc microgrid with hybrid storage system," Proc. of IEEE First International Conference on DC Microgrids, pp. 62–68, Jun. 2015.

[5] A. M. Dizqah, A. Maheri, K. Busawon, and A. Kamjoo, "A multivariable optimal energy management strategy for standalone dc microgrids," IEEE Trans. on Power Systems, vol. 30, no. 5, pp. 2278–2287, Sep. 2015.

[6] A. Werth, N. Kitamura, and K. Tanaka, "Conceptual study for open energy systems: distributed energy network using interconnected dc nanogrids," IEEE Trans. on Smart Grid, vol. 6, no. 4, pp. 1621–1630, Jul. 2015.

[7] C. Wang, X. Li, L. Guo, and Y. W. Li, "A nonlinear-disturbance-observer-based dc-bus voltage control for a hybrid ac/dc microgrid," IEEE Trans. on Power Electronics, vol. 29, no. 11, pp. 6162–6177, Nov. 2014.

[8] C. Zhao, S. Dong, F. Li, and Y. Song, "Optimal home energy management system with mixed types of loads," CSEE Journal of Power and Energy Systems, vol. 1, no. 4, pp. 29–37, Dec. 2015.

[9] S. Lim, J. Ranson, D. M. Otten, and D. J. Perreault, "Two-stage power conversion architecture suitable for wide range input voltage," IEEE Trans. on Power Electronics, vol. 30, no. 2, pp. 805–816, Feb. 2015.

[10] S. Guo, Y. Gao, Y. Xu, X. Lin-shi, and B. Allard, "Digital PWM controller for high-frequency low-power DC-DC switching mode power supply," Proc. of IEEE International Power Electronics and Motion Control Conference, pp. 1340–1346, May 2009.

[11] A. Costabeber, P. Mattavelli, S. Saggini, and A. Bianco, "Digital autotuning of DC-DC converters based on a model reference impulse response," IEEE Trans. on Power Electronics, vol. 26, no. 10, pp. 2915–2924, Oct. 2011.

[12] Z. Shen, N. Yan, and H. Min, "A multimode digitally controlled boost converter with PID autotuning and constant frequency/constant off-time hybrid PWM control," IEEE Trans. on Power Electronics, vol. 26, no. 9, pp. 2588–2598, Sept. 2011.

[13] V. Arikatla and J. a. Abu Qahouq, "An adaptive digital PID controller scheme for power converters," Proc. of IEEE Energy Conversion Congress and Exposition, pp. 223–227, Sept. 2010.

[14] M. Shirazi, R. Zane, and D. Maksimovic, "An autotuning digital controller for dc-dc power converters based on online frequency-response measurement," IEEE Trans. on Power Electronics, vol. 24, no. 11, pp. 2578–2588, Nov. 2009.

[15] Y. Furukawa, S. Hirotaki, S. Watanabe, F. Kurokawa, N. Matsui and I. Colak, "A consideration of transient response for sensorless model control dc-dc converter," Proc. of IEEE International Telecommunications Energy Conference, pp. 936-941, Oct. 2015.

[16] K. Kajiwara, H. Tajima, F. Kurokawa, "Wide input and load integral gain changeable digital control dc-dc converter," International Journal of Renewable Energy Research, vol. 5, no. 4, pp. 1212-1219, Dec. 2015.

[17] H. Matsuo, F. Kurokawa, and K. Higashi, "Dynamic characteristics of the digitally controlled dc-dc converter," IEEE Trans. on Power Electronics, vol. 4, no. 4, pp. 419–426, Oct. 1989.